Cell Reports
Sustainability

Article

# The warming effect of black carbon must be reassessed in light of observational constraints

## Highlights

- We constrain warming estimates by BC using recent observations and emission inventories
- We find BC warming due to aerosol-radiation interaction spans a factor of three
- Rapid atmospheric adjustments reduce the instantaneous radiative forcing by nearly 50%

## Authors

Gunnar Myhre, Bjørn H. Samset, Camilla Weum Stjern, ..., Drew Shindell, Philip Stier, Duncan Watson-Parris

## Correspondence

gunnar.myhre@cicero.oslo.no

## In brief

Warming from BC stays uncertain despite observational constraints.

Myhre et al., 2025, Cell Reports Sustainability *2*, 100428
September 26, 2025 
https://doi.org/10.1016/j.crsus.2025.100428

CellPress

Please cite this article in press as: Myhre et al., The warming effect of black carbon must be reassessed in light of observational constraints, Cell Reports Sustainability (2025), https://doi.org/10.1016/j.crsus.2025.100428

Cell Reports Sustainability

CellPress
OPEN ACCESS

Article

# The warming effect of black carbon must be reassessed in light of observational constraints

Gunnar Myhre,[1,13,*] Bjørn H. Samset,[1] Camilla Weum Stjern,[1] Øivind Hodnebrog,[1] Ryan Kramer,[2] Chris Smith,[3,4] Timothy Andrews,[5] Olivier Boucher,[6] Greg Faluvegi,[7,8] Piers M. Forster,[3] Trond Iversen,[9] Alf Kirkevåg,[9] Dirk Olivié,[9] Drew Shindell,[10] Philip Stier,[11] and Duncan Watson-Parris[12]

[1]CICERO Center for International Climate Research, Oslo 0318, Norway
[2]NASA Goddard Space Flight Center, Earth Sciences Division, Greenbelt, MD, USA
[3]School of Earth and Environment, University of Leeds, Leeds, UK
[4]International Institute for Applied Systems Analysis (IIASA), Laxenburg, Austria
[5]Met Office Hadley Centre, Exeter, UK
[6]Institut Pierre-Simon Laplace, Sorbonne Université/CNRS, Paris, France
[7]Center for Climate System Research, Columbia University, New York, NY, USA
[8]NASA Goddard Institute for Space Studies, New York, NY, USA
[9]Norwegian Meteorological Institute, Oslo, Norway
[10]Nicholas School of the Environment, Duke University, Durham, NC, USA
[11]Department of Physics, University of Oxford, Atmospheric, Oceanic and Planetary Physics, Oxford, UK
[12]Scripps Institution of Oceanography and Halicioğlu Data Science Institute, University of California, San Diego, La Jolla, CA, USA
[13]Lead contact
*Correspondence: gunnar.myhre@cicero.oslo.no
https://doi.org/10.1016/j.crsus.2025.100428

**SCIENCE FOR SOCIETY** Incomplete combustion of fossil fuels, biofuels, and biomass leads to emissions of black carbon (BC). BC adversely impacts air quality and contributes to climate change. The climate effect of BC has been debated for decades and remains much more uncertain than that of greenhouse gases. This is due to its inhomogeneous distribution in the atmosphere; uncertainties in how strongly it absorbs sunlight; and its complex influence on temperature, water vapor, and clouds.

We use observational constraints and four climate models to uncover a factor of three difference in surface temperature response to BC-induced warming. This, combined with recent satellite-based information, highlights the need for a community effort to evaluate climate models against a broader set of observations in order to reduce the uncertainty associated with the climate impact of BC.

## SUMMARY

Anthropogenic emissions of black carbon (BC) aerosols are generally thought to warm the climate. However, the magnitude of this warming remains highly uncertain due to limited knowledge of BC sources; optical properties; and atmospheric processes such as transport, removal, and cloud interactions. Here, we assess and constrain estimates of the historical warming influence of BC using recent observations and emission inventories. Based on simulations from four climate models, we show that the current global mean surface temperature change from anthropogenic BC due to aerosol-radiation interaction spans a factor of three—from +0.02 ± 0.02 K to +0.06 ± 0.05 K. Rapid atmospheric adjustments reduce the instantaneous radiative forcing by nearly 50% (multi-model mean), substantially lowering the net warming. Yet, recent satellite constraints suggest a stronger effect, highlighting the need for a more comprehensive reassessment of BC's climate influence.

## INTRODUCTION

Atmospheric black carbon (BC) aerosols, emitted from incomplete combustion of fossil fuel, biofuel, and biomass burning, can both scatter and absorb incoming solar radiation.[1–4] Anthropogenic BC emissions are generally thought to exert a positive net radiative forcing and were assessed by the Intergovernmental Panel on Climate Change ( IPCC) 6th Assessment Report

Please cite this article in press as: Myhre et al., The warming effect of black carbon must be reassessed in light of observational constraints, Cell Reports Sustainability (2025), https://doi.org/10.1016/j.crsus.2025.100428



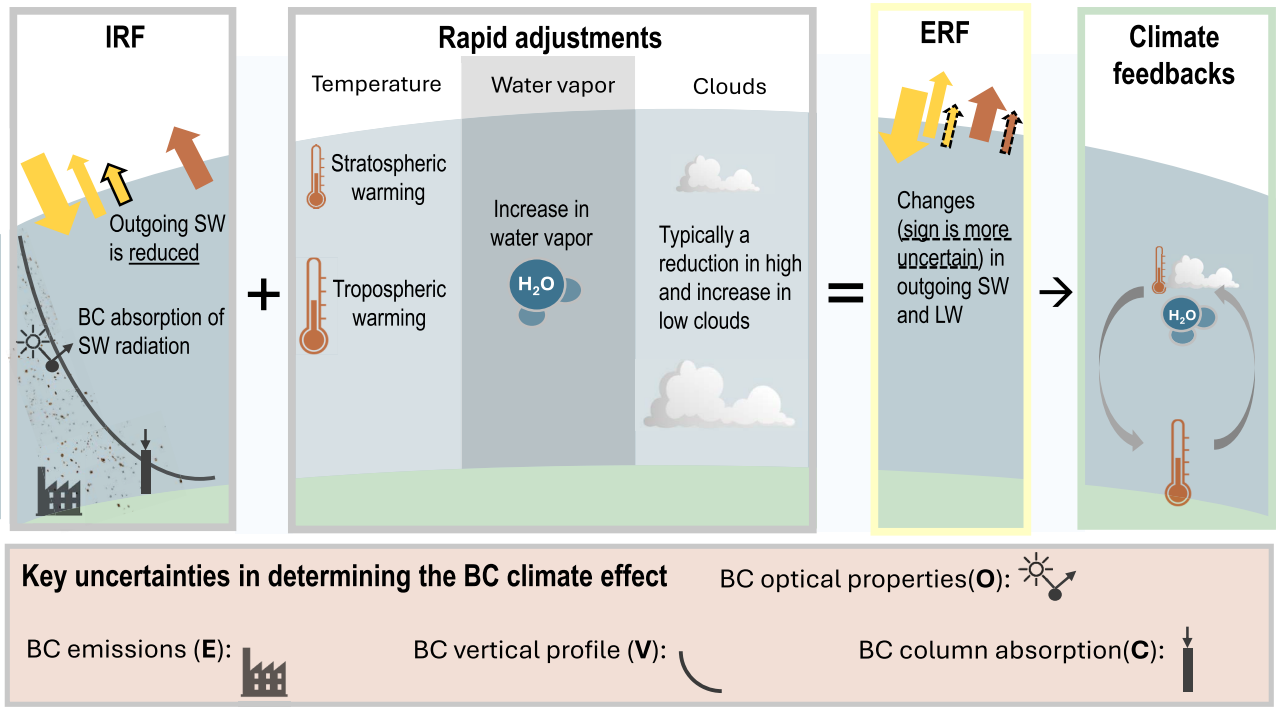


**Figure 1. Illustration of BC impact on climate**

Schematic illustration of the instantaneous change in top-of-the-atmosphere radiative fluxes, rapid adjustments, and feedback processes. Yellow arrows are for shortwave radiation and red for longwave radiation. The thinnest lines (one for shortwave and one for longwave) are perturbations to the radiation budget by BC.

(AR6) to be currently (year 2019) responsible for 0.07°C of global annual mean surface warming.[5]

This estimate is, however, highly uncertain, and has varied strongly in recent assessments due to a range of factors that are challenging both to observe and to represent in global climate models. These include the efficiency of the direct interaction of BC with sunlight, notably how strongly it absorbs radiation and transfers the energy to the surrounding air; the change of BC concentrations with altitude, which affects its warming because absorption is more efficient above a high albedo surface such as a cloud[1]; the transport, aging, and removal mechanisms of BC aerosols; and the overall amount of anthropogenic BC emissions. Further, although the energy absorption by BC occurs almost entirely in the solar spectrum, the resulting atmospheric heating triggers responses with impacts also on thermal infrared radiation.[6] These so-called rapid adjustments (RAs) include changes in atmospheric temperature,[7,8] in water vapor concentration,[7,8] and to cloud formation and properties.[9,10] RAs are initiated within hours after a BC particle is emitted[11] and have recently been shown to be critical in determining the total influence of absorbing aerosols on the atmospheric energy budget.[8,12–14]

In the current study, we present a set of climate model simulations, and a range of scaling exercises, to quantify the influence of these key uncertainties on estimates of the climate influences of BC emissions. First, however, we illustrate and discuss the current understanding of the progress from the emission of a BC particle, through to its influence on surface temperatures, and where the key uncertainties come in (see Figure 1).

The first important factor is the absolute volume of emissions, which varies among available datasets.[15,16] Observations indicate a reduction of global BC emissions in recent years, with a current best estimate of around 4.9 Tg $yr^{-1}$.[17] Recent modeling exercises, such as Coupled Model Intercomparison Project Phase 6 (CMIP6),[18] have generally used higher emissions than previous multi-model exercises,[19] leading to challenges in comparing modeling studies over time. Naturally, misrepresenting the level of emissions will influence the estimate of the climate effect of BC. In addition, the so-called representativeness error, where measurements of the BC concentrations close to an emission site are taken to be representative of a large, coarse climate model grid box when tuning climate models, has been shown to result in a positive bias.[20]

Next, we need to know how far, and how high up, BC particles are transported after emission. In recent modeling studies, the concentration of BC in the middle and upper troposphere is typically lower than in the previous generation of global aerosol models.[21–23] This has been related to the lifetime of BC, which is, in turn, primarily related to how models age the particles after emission and how effectively the particles are removed by precipitation. Comparisons with observations indicate that the CMIP5 generation of global models overestimated the concentrations of BC in the upper troposphere, likely leading to elevated radiative forcing due to the increased forcing efficiency with altitude.[24]

We also need to know the absorptive properties of BC, which are typically quantified by the mass absorption coefficient

Please cite this article in press as: Myhre et al., The warming effect of black carbon must be reassessed in light of observational constraints, Cell Reports Sustainability (2025), https://doi.org/10.1016/j.crsus.2025.100428





**Table 1. BC experiments, their temperature response, and description.**

| Experiments | Global mean ΔT | Description of constraint/scaling |
|---|---|---|
| BC-E | 0.05 ± 0.02 | Scaled to account for updated emission inventories. |
| BC-EVO | 0.02 ± 0.02 | In addition to the emission scaling (E), BC profiles are vertically (V) constrained prior to simulation by reducing models' BC lifetime to better match observed BC profiles. Constraining the optical properties (O) by scaling MAC. |
| BC-EVOC | 0.06 ± 0.05 | In addition to the EV constraint, responses are further scaled to satellite data of column (C) absorption by BC. This scaling is vertically uniform and thus only constitutes an increased magnitude of BC-EVO responses. |
| IPCC AR6 | 0.07 | Central estimate from the latest IPCC report. |

Temperature change numbers are averages over all four models. As all experiments as based on BC×10 simulations (see Methods), all responses are scaled so that they represent responses to a BC concentration increase corresponding to the increase from preindustrial until present day. Further, all responses are scaled to account for updated knowledge of the typical optical properties of BC. See Methods and Figure 1.

(MAC). The MAC magnitude is crucial for the BC radiative effect[19] and has been measured to be, on average, around 7.5 ± 1.2 $m^2\ g^{-1}$ (at 550 nm) for freshly generated particles.[3] MAC is, however, enhanced when BC particles age and are coated by non-BC aerosols. The efficiency of non-BC aerosols in enhancing the absorption of BC is debated,[25–27] but most recent observations, taking low-volatility organics into account, indicate an aged MAC of around 10 $m^2\ g^{-1}$ (at 550 nm).[27] However, the aging enhancement factor depends on the morphology assumption on the BC core,[28] and the average enhancement over time and space is uncertain.[29] Table S1 shows a range of measurements of MAC, illustrating a substantial range, likely due to regional differences and different measurements techniques.[30] Meanwhile, global models have shown a tendency to underestimate the MAC by about 25%–50%[31] compared with regional measurements.[30]

In all, the emissions, geographical distribution, vertical profile, and MAC broadly determine the instantaneous forcing (IRF) of BC aerosols (left panel in Figure 1). This is, however, where the RAs come in, altering the net influence of BC on the energy balance. For instance, based on idealized experiments with CMIP5 generation models, Smith et al.[8] showed RAs to be strongly negative for BC, with cloud changes as one of the main contributors. Whether the cloud response enhances or counteracts the direct influence on the radiation budget, however, differs between various studies.[19,32] The sign of the BC influence on clouds is mainly dependent on whether BC is located above or below clouds,[33–35] whereas the strength of the impact depends on atmospheric conditions and cloud properties.[34] Available estimates of BC-induced cloud changes come from models with spatial resolutions ranging from hundreds of kilometers (global scale models) to tens of meters (large eddy simulations)[32,35,36] and are partly based on satellite retrievals.[37,38]

After RAs, the remaining net influence of BC on the global energy balance is termed the effective radiative forcing (ERF).[19,39,40] ERF has been found to be more directly related to subsequent surface temperature change than IRF. For BC, ERF is typically found to be markedly lower than IRF due to the RAs (see results below); this insight is one reason the estimated relative importance of BC in anthropogenic climate change was markedly lower in the IPCC AR6 (0.07 C, based on an ERF estimate) than in the AR5 (which used IRF estimates but did not give a temperature estimate for BC separately).

In this study, we use a set of recent modeling studies, combined with observational constraints, to provide a revised estimate for the influence of current anthropogenic BC emissions on global annual mean surface temperature. Our main aim is to illustrate the individual and combined importance of a set of three uncertainties: the level of emissions, the vertical profile of BC in the atmosphere, and the total amount of shortwave absorption stemming from the MAC of aged BC. We also discuss how our revised estimates compare to previous and more recent estimates from the IPCC. Our results are based on four climate models with BC responses that are initially typical of the previous CMIP5 generation of global models. Some of these simulations are already thoroughly documented in previous studies.[8,31,41] Here, we scale these results to match recent emission estimates and then compare the responses to new simulations, where the vertical profile of BC has been constrained by observations in the upper troposphere as well as recent constraints based on satellite data of column absorption by BC (see Methods). Our best estimates of ERF and surface temperature change of BC from aerosol-radiation interactions are both lower than those arrived at in IPCC AR6, and we conclude by discussing the reasons for, and implications of, this result.

## RESULTS

The model experiments used in this paper, and the scalings to observational constraints, are summarized in Table 1 and described in full in Methods. Briefly, we have three sets. BC-E denotes simulations from four models (ECHAM-HAM-M7, GISS-E2, NCAR-CESM-CAM4, and NorESM1) where BC concentrations (or, in one case, emissions) have been increased by 10x. These have previously been analyzed as part of the Precipitation Driver Response Model Intercomparison Project (PDRMIP).[31] Relative to the PDRMIP 10 model mean, two of our current models showed high sensitivity to BC emissions and two showed weak sensitivity (see further discussion in the Supplement). Here, in BC-E, we have scaled these results to reflect the most updated emission inventories of anthropogenic BC (4.9 Tg $yr^{-1}$; CEDS v2024.04.01).[17]

Next, in BC-EVO, we have performed additional 10× BC experiments with the same models but where the vertical profile (V) of BC has been tuned to match updated knowledge on

Please cite this article in press as: Myhre et al., The warming effect of black carbon must be reassessed in light of observational constraints, Cell Reports Sustainability (2025), https://doi.org/10.1016/j.crsus.2025.100428



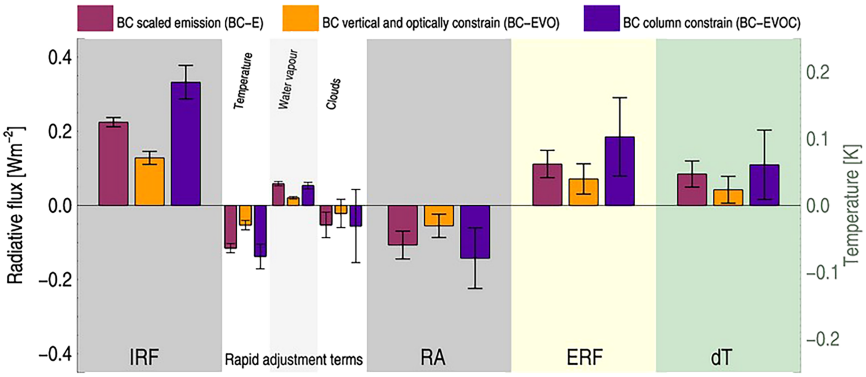


**Figure 2. Forcing and temperature change due to BC**

Calculated global mean values from the three experiments, BC-E, BC-EVO, and BC-EVOC, showing instantaneous radiative forcing (IRF), rapid adjustments (RAs), effective radiative forcing (ERF), and surface temperature change (dT). Surface temperature change has a y axis on the right-hand side. Uncertainty ranges are taken as one standard deviation among the four climate models. All three experiments are scaled to current BC inventories, see further description in Table 1.

abundancies in the upper vs. lower troposphere.[21,22] This is done by either prescribing a BC concentration distribution from a model with tuned BC removal or by tuning the removal in the model itself (ECHAM); see Methods. In addition, we have scaled the simulations to match observations of optical properties (O) of BC, specifically the MAC, as the observed value of 10 $m^2$ $g^{-1}$ is higher than the multi-model mean of this study (7.3 $m^2$ $g^{-1}$ ± 10% at 550 nm).

Finally, in BC-EVOC, we have applied a scaling to make the column average (C) absorbing aerosol optical depth (AAOD) match the recent satellite-based constraint by Chen et al.[42] Taken together, these three experiments represent a stepwise constraining of model results to match the current best estimates of the three key uncertainties in the quantification of the surface temperature impacts of BC emissions.

Figure 2 shows the IRF, RA, and ERF from all experiments, calculated as a combination of direct model output, double radiation calls, and application of radiative kernels, following Myhre et al., Smith et al., and Soden et al.[8,43,44] The global annual mean temperature change is also shown, quantified from fully coupled climate model simulations, as a mean over the years 51–100 after the 10× BC perturbation is applied.

In BC-E, we find a surface temperature change for current anthropogenic BC emissions of 0.05 (±0.02) °C, where the standard deviation is taken across the four models. We note that this gives the same relative standard deviation as using the full set of 10 PDRMIP models that performed the BC×10 experiment (see Table S2). This temperature influence is lower than the 0.07°C assessed by IPCC AR6[5] but consistent within errors; we discuss this further below.

In BC-EVO, where the vertical profile and optical parameters are constrained, we find a markedly lower temperature influence of 0.02 (±0.02) °C. This is mainly due to the lower BC total abundance in the upper troposphere, where its absorption is particularly efficient.[45–47] For example, Sand et al.[48] demonstrate, using two climate models, that IRF of BC is 2–3 times stronger in the upper troposphere compared with the lowest 2 kilometers of the atmosphere. We note that the IRF of 0.33 $Wm^{-2}$ in BC-EVOC is 50% higher than BC-E and is identical to the estimate in Chen et al.,[42] even though we take into account the lower recent BC emissions over the last decade, as opposed to Chen et al.[42]

Finally, in BC-EVOC, we find a warming influence from BC of 0.06 (±0.05) °C. The strong increase here is because the satellite-derived constraint on BC AAOD from Chen et al.[42] is markedly higher than what is simulated by most models.

In Figure 3, we show the geographical distributions of the multi-model mean surface temperature change, displaying a strongly inhomogeneous pattern. Reflecting the proximity to the BC emission sources, the warming is much stronger in the Northern Hemisphere than the Southern Hemisphere—and stronger over continents than over oceans. However, many of the regions that have a high abundance of BC, such as Southeast Asia, show a very modest warming, or even a

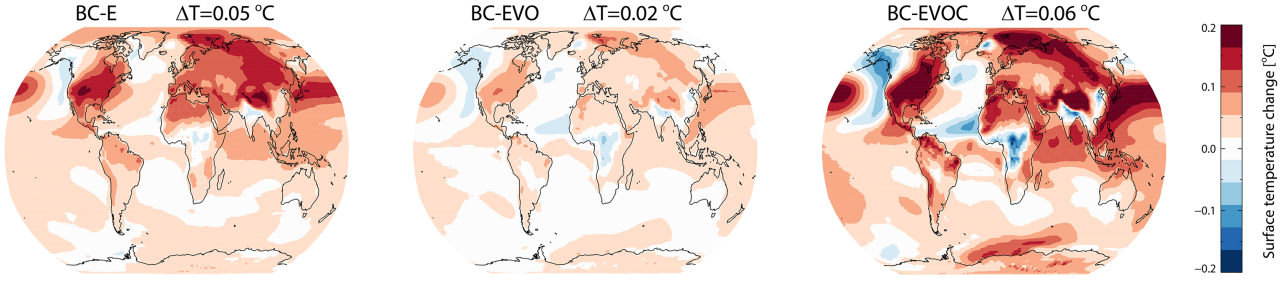


**Figure 3. Temperature change due to BC**

Multi-model annual mean surface temperature change for the BC-E, BC-EVO, and BC-EVOC experiments. The change is relative to model PDRMIP reference simulation.[49]

Please cite this article in press as: Myhre et al., The warming effect of black carbon must be reassessed in light of observational constraints, Cell Reports Sustainability (2025), https://doi.org/10.1016/j.crsus.2025.100428





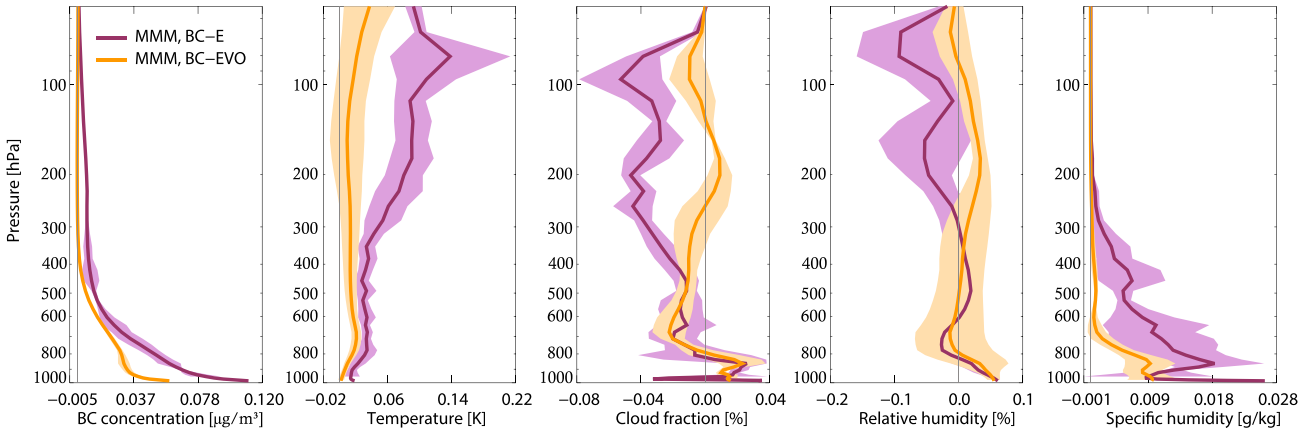


**Figure 4. Global mean vertical profile and BC-induced changes**

Atmospheric vertical profiles of changes in BC concentration, temperature, cloud fraction, and relative and specific humidity for the two experiments, BC-E and BC-EVO, from the fsst simulations. The model diversity is shown by the shading given as one standard deviation among the models.

cooling, suggesting the presence of compensating effects. The geographical pattern of warming is similar in BC-E and BC-EVO, even though the vertical and horizontal BC distributions are quite different. Note that BC-EVOC has an identical warming pattern to BC-EVO, as it only includes an additional column absorption scaling that enhances the magnitude of the response.

In Figure 4, we show the atmospheric vertical profiles of change in BC concentration (for individual models in Figure S1), temperature, cloud fraction, and relative and specific humidity. (BC-EVOC is omitted as it has the same profile as BC-EVO.) The profiles are markedly different in the upper troposphere for all models, where the unconstrained BC-E simulation shows strong changes whereas BC-EVO has almost none. In the lower troposphere, temperature changes and cloud changes are relatively similar for the two simulations. The cloud fraction changes largely follow the relative humidity profile. Specific humidity changes are positive throughout the troposphere, with much stronger increases in BC-E than in BC-EVO. The model diversity (shown as one standard deviation) is larger for BC-E than BC-EVO but varies vertically and is generally low for cloud changes. No particular model dominates the model spread, except for temperature changes around 100 hPa in BC-E, where NCAR-CESM1-CAM4 has a much larger temperature increase than the three other models (Figure S2).

BC typically reduces cloud cover in altitudes where it is present while increasing cloud cover at lower heights. This dynamic leads to a strong negative adjustment when BC is in the upper troposphere, characterized by a reduction in high clouds and an increase in middle and lower clouds.[48] In the BC-E experiment, the RA due to clouds is similar in magnitude to the sum of the other RA terms. For the BC-EVO and BC-EVOC experiments the RA of clouds is 40% of the total RA in a multi-model mean. Earlier studies have focused primarily on BC RA due to clouds,[32] but our results illustrate the importance of including all RA terms. We note, however, that the cloud RA has a strong inter-model standard deviation and is even positive in one of the models. The models used for the IPCC AR6 assessment also showed a large range in cloud adjustment, spanning strongly negative to slightly positive values.[50]

We find that the total RAs are negative in all three experiments. Recall that although the IRF quantifies the radiative impact only, the ERF incorporates the RAs and is thus sensitive to the magnitude of these adjustments. The negative RA of BC involves changes in (land) surface, tropospheric, and stratospheric temperatures caused by the atmospheric heating by BC, which increases the longwave radiation to space (Planck feedback). See further discussion in Smith et al.[8] on the impact on longwave radiation and how this differs among climate drivers. Water vapor change is a positive RA resulting from increased atmospheric temperatures. For BC-E the RA contributes to lowering the ERF by 50% relative to the IRF. For BC-EVO and BC-EVOC, the RA causes a 43% reduction from IRF to ERF (see Supplementary Note S1 and Figure S3 for split into longwave and shortwave contributions). In addition to the atmospheric RA terms, the prescribed sea-surface temperature simulations used to quantify ERF show small land surface temperature and albedo changes. We also note that Figure 2 shows a particularly strong change in the cloud RA between the BC-E and BC-EVOC experiments, indicating that cloud changes in the middle and upper troposphere are especially important.

Recently, the IPCC AR6 provided an updated estimate of the present-day climate warming due to BC emissions[50] of 0.07°C. This estimate was based on simulations, with a change in BC emission representative of a change between preindustrial and current conditions and simulated for 30 years. In the simulations, the CEDS v2016.07.16 (CMIP6 release) were used for year 2014, and these emissions are more than 50% higher compared with CEDS v2024.04.01 for year 2022. However, Forster et al.[51] showed that effective radiative forcings weaker than 0.1 $Wm^{-2}$ involve large uncertainties in 30-year simulations because the signal is weak compared with natural variability. For several of the models involved in Thornhill et al.,[50] the ERF was weak and thus uncertainties in the ERF of BC are substantial.

In this study, we have chosen to base our analyses on strong 10-fold increases in BC, which we have thereafter scaled to

Please cite this article in press as: Myhre et al., The warming effect of black carbon must be reassessed in light of observational constraints, Cell Reports Sustainability (2025), https://doi.org/10.1016/j.crsus.2025.100428



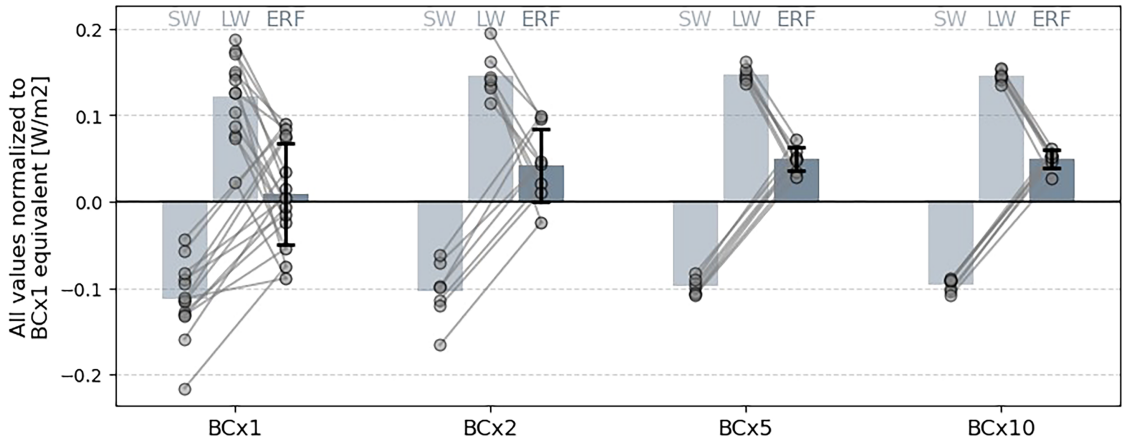


**Figure 5. Linearity of BC ERF**

Illustration of linearity of BC perturbations in simulations using CESM2-CAM4 with original (BC-E) profiles. Bars show the mean normalized shortwave (SW), longwave (LW), and net ERF for 200-year simulations with industrial era BC (BC×1) and 100-year simulations with twice the industrial era BC (BC×2), five times the industrial era BC (BC×5), and ten times the industrial era BC (BC×10), respectively. Circles show consecutive 15-year mean values, with lines connecting individual 15-year SW and LW values with the corresponding ERF value. Whiskers on ERF bars indicate +/− one standard deviation.

match the preindustrial to present-day increase in BC. We believe this method is more reliable for relatively short simulations of small perturbations and have performed an additional set of sensitivity simulations to illustrate this point. Figure 5 shows ERF of simulations, using one of the models, with industrial era BC (BC×1), industrial era BC multiplied by two (BC×2), five (BC×5), and ten (BC×10). The ERFs are normalized by the BC industrial era BC abundance to investigate the linearity of BC perturbation. The simulations were run for 100 years with fixed sea-surface temperatures for BC×2, BC×5, and BC×10 and for 200 years for BC×1. The bars indicate the mean over the full simulations, whereas the circles indicate all of the consecutive 15-year period included in the full simulations. The normalized mean full ERFs are very similar in the BC×2, BC×5, and BC×10, but the spread of the circles indicates reduced variability as the perturbation becomes stronger. In the BC×1 simulation, the 15-year means vary widely, ranging from negative to positive values. The forcing perturbation in BC×1 is weak compared with the internal variability, and very long simulations are required to get a representative ERF. Overall, the figure shows that the ERF exerted by BC is linear in concentration, up to ten times the change over the industrial era. This supports findings in Hodnebrog et al.[45] and validates our methodology of performing strong perturbations that are later scaled to match present-day levels. Consequently, we find that the AR6 estimate of historical era BC-induced warming may have had marked uncertainty and is fully consistent with the range of lower estimates we present here.

## DISCUSSION

We have shown that estimates of climate impacts of BC vary strongly in the literature and that uncertainties in the climate effect of BC are particularly associated with emissions, atmospheric residence time (and thus the resulting vertical distribution), and optical properties such as absorption.[3,19,52]

BC emission data have previously been assessed to have a factor of two uncertainty.[53] We have mentioned the transition between emissions typically used in previous multi-model assessments (v2016.07.16 BC emissions CEDS[16]) compared with the most recent version of the CEDS data (v2024.04.01) used in newer studies. Although the most recent CEDS data have 8% higher emissions than older generations of multi-model studies, the previous CEDS version is 66% higher, partly because of higher emissions in 2,000 and partly as a result of an increase in BC emissions since 2,000. The lower discrepancy for the most recent CEDS version is mainly caused by a revisiting of emission before 2014 and a continued reduction after 2014. Although all our estimates are scaled to current emissions from CEDS, Zhao et al. (2024)[54] show that an earlier version of CEDS and other bottom-up emission inventories most likely underestimate BC emissions over China compared with a top-down approach. However, there are several limitations associated with the top-down approach, and more research is needed to robustly conclude that Chinese BC emissions are underestimated. In our analyses we scale the results to match the most recent CEDS emission. To illustrate the importance of that scaling, we show in Table S3 responses in ERF, IRF, and RAs for both versions 2024.04.01 and 2016–07.16.

We have also shown ERF due to BC over the industrial era to be lower than IRF (the direct BC aerosol effect) by around 50% in the multi-model mean. ERF has previously been found to be the most representative way to compare the surface temperature change from a perturbation to the Earth's energy budget for different climate drivers, including BC.[39] The total RA due to BC is strongly negative, and recent findings[8] underline the importance of atmospheric temperature increase and a negative cloud RA. Despite some model diversity in the IRF and in the magnitude of the cloud RA, we have found that, overall, the RA and ERF are consistent among four climate models, as are the underlying physical processes of vertical changes in

atmospheric temperature, water vapor, and clouds. This consistency includes simulations from three climate models using concentration fields of BC, and one model used emissions to derive the BC atmospheric concentration.

Note that the temperature change from the fully coupled climate model simulations is taken as a mean over the years 51–100. This means that our temperature response estimates are likely overstated compared with the current temperature change due to present-day anthropogenic BC because the model has had many decades to respond to the current levels, including a component from the deep ocean, unlike the real world. Therefore, we consider this an upper-bound from the four models. A lower bound, found by using a 5-year mean around year 20, is about 20% weaker than our upper-bound (see supplementary text for further discussion).

In conclusion, we find that there is a need for further work to provide an up-to-date estimate of the influence of anthropogenic BC emissions on global surface temperature over the historical era. Such efforts should ensure consistent treatment of emissions, and adherence to observational constraints of the vertical profile of BC in the atmosphere, its optical properties, and the total amount of absorption by BC in current satellite estimates.

## METHODS

### Concepts

#### *IRF—instantaneous radiative forcing*

The immediate energy imbalance at the top-of-atmosphere (TOA) caused by direct interactions between changed atmospheric BC burden and radiation, positive for increased energy input to the earth system.

#### *RA—rapid adjustments*

The short-term adjustments of atmospheric properties to the IRF that are not due to responses to surface temperature changes.

#### *ERF—effective radiative forcing*

The TOA radiative energy perturbation is due to the combination of IRF and the RAs. Thus, the TOA perturbation after RAs have taken place is positive for the increased energy input to the earth system.

#### *Climate response*

Any changes in climate variables in response to ERF, including the deep oceans. Ideally, a full climate response to an imposed ERF is the difference between climate states in long-term equilibrium, with and without the imposed ERF. The high inertia of the deep oceans hampers such estimates in practice. Instead, a *Transient Climate Response* is estimated after a given time for partial adjustment; in this case, we use 100-year-long coupled simulations.

#### *Models*

This study uses a subset of 4 PDRMIP models out of 10 Precipitation Driver Response Model Intercomparison Project (PDRMIP) models.[49] We use simulations from the four global climate models ECHAM-HAM-M7, GISS-E2-R, NCAR-CESM-CAM4, and NorESM1. In PDRMIP, atmosphere-land simulations with prescribed sea-surface temperatures (*AMIP-type*) and fully atmosphere-land-ocean-coupled (*CMIP-type*) simulations are applied for a large set of climate drivers and a reference simulation representing current climate conditions. The models include the atmospheric effect of absorption and scattering of BC but do not include any aerosol-cloud interactions and BC effect on snow and ice (with the exception of NorESM1, which includes the BC effect on snow and ice). For a further description of the PDRMIP models see Myhre et al.[49]

#### *Simulations*

The anthropogenic BC is scaled to its atmospheric change during the industrial era. Prescribed concentration fields are imported in three of the models (GISS, NCAR-CESM-CAM4, and NorESM1), which are thus run concentration driven without feedback between climate variables and BC concentrations. The fourth model (ECHAM) calculates BC concentrations from emissions and thus allows feedback between BC and atmospheric variables. Both 15-year-long AMIP-type (fixed sea-surface temperature) and 100-year-long CMIP-type simulations are performed (see also Supplementary Note S2).

Each model produces a standard set of climate response experiments (**BC-E**) based on importing BC data from the BC×10 (BC concentrations/emissions multiplied by 10) core set of PDRMIP simulations, see Figure S4 for ERF and Figure S5 for surface temperature change. Imported concentration fields in BC-E are multi-model mean fields from AeroCom.[52] A new set of simulations (**BC-EVO**) are performed by importing (in GISS, NCAR-CESM-CAM4, and NorESM1) or producing (in ECHAM) lifetime-adjusted BC×10 data to constrain the concentration profile to observations. We use a single model field for imported BC concentrations in the BC-EVO experiment.[45] The BC overabundance in the upper troposphere is reduced by increasing the wet removal of BC, which results in a shorter lifetime. Various sensitivity simulations are performed in Hodnebrog et al.[45] to achieve a realistic agreement with the aircraft measurements. In this study, the PERTBC simulation in Hodnebrog et al.[45] is adopted, but emissions are as in the standard case in Hodnebrog et al.[45] The vertical profiles for BC STD and BC-EVO are shown in Figure S1. The lifetime of BC in BC-EVO for the models GISS, NCAR-CESM-CAM4, and NorESM1 is 3.9 days[45] compared with 7.4 days in BC-E.[31] In the emission-driven simulations in ECHAM-HAM the wet removal tendencies of BC are scaled by a factor of 2, resulting in a change in the lifetime from 7.4 days (in BC-E) to 3.7 days (in BC-EVO). In **BC-EVOC**, we further scale the BC-EVO simulation with the ratio of absorption aerosol optical depth based on satellite data[42] of 0.0044 (550 nm) to 0.0017 (550 nm) in BC-EVO.

In the BC-E PDRMIP experiment, the four selected models have a mean ERF within 1% of the mean of the 10 PDRMIP models, whereas the number is 25% lower for surface air temperature change.

#### *Results after constraining to the observed MAC and emission data*

All results are scaled to best match current BC emission estimates using the Community Emission Data System (CEDS) version 2024.04.01.[17] The CMIP6 BC emission in CEDS (version 2016.07.16) is 66% larger (from 4.6 to 7.6 Tg $yr^{-1}$) than the emissions used in AeroCom dataset (BC STD experiment) due to a strong increase in recent years and overall improved estimation of BC sources.[16] However, the most recent version of the CEDS data (version 2024.04.01) has only 8% (from 4.6 to 4.9 Tg $yr^{-1}$) higher emissions than used in previous multi-model studies.

This is mainly caused by a revisiting of emissions before 2014 and a continued reduction after 2014. In all Figures and numbers, the most recent CEDS data are used. In the Table S3, we report results from BC emissions of 4.9 and 7.6 Tg $yr^{-1}$. The concentration field applied in the BC-EVO experiment is derived from the EU project ECLIPSE emission dataset,[55,56] with a total BC emission of 7.1 Tg $yr^{-1}$ (5.5 and 1.6 Tg $yr^{-1}$, respectively, from anthropogenic and natural sources).

Observations of MACs vary strongly,[3,30] see Table S1. Models have typically lower MAC values than observations. The mean MAC among the four models applied in this study is 7.3 $m^2$ $g^{-1}$ ± 10% (550 nm). We scale this value to 10 $m^2$ $g^{-1}$ (550 nm), which we find to be a representative value from the selected values in Table S1.

The scaling of the results by emissions and MAC is done on all post-processed GCM output. All results in this study thus represent a change in BC from preindustrial to present-day emissions of 4.9 Tg $yr^{-1}$. Scaling of the mass absorption coefficient of 10 $m^2$ $g^{-1}$ (550 nm) is done for BC-EVO and BC-EVOC. The scaling is applied to the multi-model mean numbers.

### *Calculations of ERF and RAs*

ERF and surface temperature changes are directly derived output from the PDRMIP models, respectively, from fixed sea-surface temperature simulations (AMIP-type) and fully coupled simulations (CMIP-type). Results from fixed sea-surface temperature simulations are taken as mean of years 6–15 and results from coupled simulations as mean of years 51–100.[41] Radiative kernel simulations[44] are applied for quantifications of the individual RA terms using a mean of 5 different radiative kernels.[8,43] Three of the models have implemented double radiation calls for quantification of IRF, whereas for NorESM1, IRF is taken as the difference between ERF and RA. When IRF is directly quantified, the residuals in the kernel simulations are discussed in the text. Similarly, BC IRF almost exclusively influences the SW radiation; therefore, the residual can be derived from LW ERF and kernel calculations, see Supplementary Note S3 and Figure S6.

## RESOURCE AVAILABILITY

### Lead contact

Further information and requests for resources should be directed to, and will be fulfilled by, the lead contact, Gunnar Myhre (gunnar.myhre@cicero.oslo.no).

### Materials availability

The PDRMIP data are available through the World Data Center for Climate (WDCC) https://www.dkrz.de/up/systems/wdcc with https://doi.org/10.26050/WDCC/PDRMIP_2012-2021.

### Data and code availability

- The PDRMIP data are available through the World Data Center for Climate (WDCC) https://www.dkrz.de/up/systems/wdcc with https://doi.org/10.26050/WDCC/PDRMIP_2012-2021. A code to read and make a summary of PDRMIP data is available at GitHub: https://github.com/ciceroOslo/PDRMIP_summary_codes

## ACKNOWLEDGMENTS

G.M. was supported by the European Union's Horizon 2020 Research and Innovation Programme (CONSTRAIN project, grant agreement no. 820829) and BUDGET project grant no. 325270 funded by the Norwegian Research Council. D.W.-P. and P.S. acknowledge funding from the UK NERC CLARIFY project NE/L013479/1. P.S. additionally acknowledges support from the European Research Council (ERC) project RECAP under the European Union's Horizon 2020 Research and Innovation Programme with grant agreement no. 724602 and the European Union's Horizon 2020 Research and Innovation Programme (FORCeS) under grant agreement no. 82120. C. S. was supported by an NERC/IIASA collaborative research fellowship (NE/T009381/1). T.A. was supported by the Met Office Hadley Centre Climate Programme funded by BEIS and Defra.

## AUTHOR CONTRIBUTIONS

Conceptualization, G.M., B.H.S., C.W.S., and Ø.H.; methodology, G.M., B.H. S., C.W.S., Ø.H., R.K., C.S., T.A., O.B., G.F., P.M.F., T.I., A.K., D.O., D.S., P.S., and D.W,-P.; investigation, G.M., B.H.S., C.W.S., Ø.H., R.K., C.S., T.A., O.B., G.F., P.M.F., T.I., A.K., D.O., D.S., P.S., and D.W.-P.; writing—original draft, G. M., B.H.S., and C.W.S.; writing—review & editing, G.M., B.H.S., C.W.S., Ø.H., R.K., C.S., T.A., O.B., G.F., P.M.F., T.I., A.K., D.O., D.S., P.S., and D.W.-P.; funding acquisition, G.M., T.A., P.M.F., and P.S.; resources, G.M., B.H.S., C. W.S., Ø.H., R.K., C.S., T.A., O.B., G.F., P.M.F., T.I., A.K., D.O., D.S., P.S., and D.W.-P.

## DECLARATION OF INTERESTS

The authors declare no competing interests.

## SUPPLEMENTAL INFORMATION

Supplemental information can be found online at https://doi.org/10.1016/j.crsus.2025.100428.

Received: April 30, 2025
Revised: May 15, 2025
Accepted: May 23, 2025

## REFERENCES

1. Haywood, J.M., and Shine, K.P. (1995). The effect of anthropogenic sulfate and soot aerosol on the clear-sky planetary radiation budget. Geophys. Res. Lett. *22*, 603–606. https://doi.org/10.1029/95GL00075.
2. Bellouin, N., Quaas, J., Gryspeerdt, E., Kinne, S., Stier, P., Watson-Parris, D., Boucher, O., Carslaw, K.S., Christensen, M., Daniau, A.L., et al. (2020). Bounding Global Aerosol Radiative Forcing of Climate Change. Rev. Geophys. *58*, e2019RG000660, e2019. https://doi.org/10.1029/2019RG000660.
3. Bond, T.C., Doherty, S.J., Fahey, D.W., Forster, P.M., Berntsen, T., DeAngelo, B.J., Flanner, M.G., Ghan, S., Kärcher, B., Koch, D., et al. (2013). Bounding the role of black carbon in the climate system: A scientific assessment. JGR Atmospheres *118*, 5380–5552. https://doi.org/10.1002/jgrd.50171.
4. Chylek, P., and Wong, J. (1995). Effect of absorbing aerosols on global radiation budget. Geophys. Res. Lett. *22*, 929–931. https://doi.org/10.1029/95GL00800.
5. Forster, P., Storelvmo, T., Armour, K., Collins, W., Dufresne, J.-L., Frame, D., Lunt, D.J., Mauritsen, T., Palmer, M.D., Watanabe, M., et al. (2021). The Earth's Energy Budget, Climate Feedbacks, and Climate Sensitivity. In Clim. Change: The Physical Science Basis. Contribution of Working Group I to the Sixth Assessment Report of the Intergovernmental Panel on Climate Change.
6. Penner, J.E., Zhang, S.Y., and Chuang, C.C. (2003). Soot and smoke aerosol may not warm climate. J. Geophys. Res. *108*, 4657. https://doi.org/10.1029/2003JD003409.
7. Smith, C.J., Kramer, R.J., Myhre, G., Alterskjær, K., Collins, W., Sima, A., Boucher, O., Dufresne, J.L., Nabat, P., Michou, M., et al. (2020). Effective radiative forcing and adjustments in CMIP6 models. Atmos. Chem. Phys. *20*, 9591–9618. https://doi.org/10.5194/acp-20-9591-2020.

8. Smith, C.J., Kramer, R.J., Myhre, G., Forster, P.M., Soden, B.J., Andrews, T., Boucher, O., Faluvegi, G., Fläschner, D., Hodnebrog, Ø., et al. (2018). Understanding Rapid Adjustments to Diverse Forcing Agents. Geophys. Res. Lett. *45*, 12023–12031. https://doi.org/10.1029/2018GL079826.

9. Ackerman, A.S., Toon, O.B., Stevens, D.E., Heymsfield, A.J., Ramanathan, V., and Welton, E.J. (2000). Reduction of tropical cloudiness by soot. Science *288*, 1042–1047. https://doi.org/10.1126/science.288.5468.1042.

10. Hansen, J., Sato, M., and Ruedy, R. (1997). Radiative forcing and climate response. J. Geophys. Res. *102*, 6831–6864. https://doi.org/10.1029/96JD03436.

11. Stjern, C.W., Forster, P.M., Jia, H., Jouan, C., Kasoar, M.R., Myhre, G., Olivié, D., Quaas, J., Samset, B.H., Sand, M., et al. (2023). The Time Scales of Climate Responses to Carbon Dioxide and Aerosols. J. Clim. *36*, 3537–3551. https://doi.org/10.1175/JCLI-D-22-0513.1.

12. Quaas, J., Andrews, T., Bellouin, N., Block, K., Boucher, O., Ceppi, P., Dagan, G., Doktorowski, S., Eichholz, H.M., Forster, P., et al. (2024). Adjustments to Climate Perturbations—Mechanisms, Implications, Observational Constraints. AGU Adv. *5*, AV001144, e2023. https://doi.org/10.1029/2023AV001144.

13. Johnson, B.T., Haywood, J.M., and Hawcroft, M.K. (2019). Are Changes in Atmospheric Circulation Important for Black Carbon Aerosol Impacts on Clouds, Precipitation, and Radiation? JGR Atmospheres *124*, 7930–7950. https://doi.org/10.1029/2019JD030568.

14. Suzuki, K., and Takemura, T. (2019). Perturbations to Global Energy Budget Due to Absorbing and Scattering Aerosols. JGR Atmospheres *124*, 2194–2209. https://doi.org/10.1029/2018JD029808.

15. Wang, R., Tao, S., Shen, H.Z., Huang, Y., Chen, H., Balkanski, Y., Boucher, O., Ciais, P., Shen, G.F., Li, W., et al. (2014). Trend in Global Black Carbon Emissions from 1960 to 2007. Environ. Sci. Technol. *48*, 6780–6787. https://doi.org/10.1021/es5021422.

16. Hoesly, R.M., Smith, S.J., Feng, L., Klimont, Z., Janssens-Maenhout, G., Pitkanen, T., Seibert, J.J., Vu, L., Andres, R.J., Bolt, R.M., et al. (2018). Historical (1750–2014) anthropogenic emissions of reactive gases and aerosols from the Community Emissions Data System (CEDS). Geosci. Model Dev. *11*, 369–408. https://doi.org/10.5194/gmd-11-369-2018.

17. Hoesly, R., and Smith, S. (2024). CEDS v_2024_04_01 Release Emission (Zenodo), Data (v_2024_04_01) [Data set]. https://doi.org/10.5281/zenodo.10904361.

18. Eyring, V., Bony, S., Meehl, G.A., Senior, C.A., Stevens, B., Stouffer, R.J., and Taylor, K.E. (2016). Overview of the Coupled Model Intercomparison Project Phase 6 (CMIP6) experimental design and organization. Geosci. Model Dev. *9*, 1937–1958. https://doi.org/10.5194/gmd-9-1937-2016.

19. Boucher, O., Randall, D., Artaxo, P., Bretherton, C., Feingold, G., Forster, P., Kerminen, V.-M., Kondo, Y., Liao, H., Lohmann, U., et al. (2013). The Physical Science Basis. Contribution of Working Group I to the Fifth Assessment Report of the Intergovernmental Panel on Climate Change. Clouds and Aerosols. In Climate Change, T.F. Stocker, D. Qin, G.-K. Plattner, M. Tignor, S.K. Allen, J. Boschung, A. Nauels, Y. Xia, V. Bex, and P.M. Midgley, eds. (Cambridge University Press), pp. 571–657.

20. Wang, R., Andrews, E., Balkanski, Y., Boucher, O., Myhre, G., Samset, B. H., Schulz, M., Schuster, G.L., Valari, M., and Tao, S. (2018). Spatial Representativeness Error in the Ground-Level Observation Networks for Black Carbon Radiation Absorption. Geophys. Res. Lett. *45*, 2106–2114. https://doi.org/10.1002/2017GL076817.

21. Samset, B.H., Myhre, G., Herber, A., Kondo, Y., Li, S.M., Moteki, N., Koike, M., Oshima, N., Schwarz, J.P., Balkanski, Y., et al. (2014). Modelled black carbon radiative forcing and atmospheric lifetime in AeroCom Phase II constrained by aircraft observations. Atmos. Chem. Phys. *14*, 12465–12477. https://doi.org/10.5194/acp-14-12465-2014.

22. Schwarz, J.P., Spackman, J.R., Gao, R.S., Watts, L.A., Stier, P., Schulz, M., Davis, S.M., Wofsy, S.C., and Fahey, D.W. (2010). Global-scale black carbon profiles observed in the remote atmosphere and compared to models. Geophys. Res. Lett. *37*, L18812. https://doi.org/10.1029/2010GL044372.

23. Lund, M.T., Samset, B.H., Skeie, R.B., Watson-Parris, D., Katich, J.M., Schwarz, J.P., and Weinzierl, B. (2018). Short Black Carbon lifetime inferred from a global set of aircraft observations. npj Clim. Atmos. Sci. *1*. https://doi.org/10.1038/s41612-018-0040-x.

24. Boucher, O., Balkanski, Y., Hodnebrog, Ø., Myhre, C.L., Myhre, G., Quaas, J., Samset, B.H., Schutgens, N., Stier, P., and Wang, R. (2016). Jury is still out on the radiative forcing by black carbon. Proc. Natl. Acad. Sci. USA. *113*, E5092–E5093. https://doi.org/10.1073/pnas.1607005113.

25. Cappa, C.D., Onasch, T.B., Massoli, P., Worsnop, D.R., Bates, T.S., Cross, E.S., Davidovits, P., Hakala, J., Hayden, K.L., Jobson, B.T., et al. (2012). Radiative Absorption Enhancements Due to the Mixing State of Atmospheric Black Carbon. Science *337*, 1078–1081. https://doi.org/10.1126/science.1223447.

26. Peng, J., Hu, M., Guo, S., Du, Z., Zheng, J., Shang, D., Levy Zamora, M., Zeng, L., Shao, M., Wu, Y.-S., et al. (2016). Markedly enhanced absorption and direct radiative forcing of black carbon under polluted urban environments. Proc. Natl. Acad. Sci. USA. *113*, 4266–4271. https://doi.org/10.1073/pnas.1602310113.

27. Zhang, Y., Su, H., Kecorius, S., Ma, N., Wang, Z., Sun, Y., Zhang, Q., Pöschl, U., Wiedensohler, A., Andreae, M.O., et al. (2023). Extremely low-volatility organic coating leads to underestimation of black carbon climate impact. One Earth *6*, 158–166. https://doi.org/10.1016/j.oneear.2023.01.009.

28. Bond, T.C., Habib, G., and Bergstrom, R.W. (2006). Limitations in the enhancement of visible light absorption due to mixing state. J. Geophys. Res. Atmos. *111*, D20211. https://doi.org/10.21029/22006JD007315.

29. Andrews, E., Ogren, J.A., Kinne, S., and Samset, B. (2017). Comparison of AOD, AAOD and column single scattering albedo from AERONET retrievals and in situ profiling measurements. Atmos. Chem. Phys. *17*, 6041–6072. https://doi.org/10.5194/acp-17-6041-2017.

30. Zanatta, M., Gysel, M., Bukowiecki, N., Müller, T., Weingartner, E., Areskoug, H., Fiebig, M., Yttri, K.E., Mihalopoulos, N., Kouvarakis, G., et al. (2016). A European aerosol phenomenology-5: Climatology of black carbon optical properties at 9 regional background sites across Europe. Atmos. Environ. *145*, 346–364. https://doi.org/10.1016/j.atmosenv.2016.09.035.

31. Stjern, C.W., Samset, B.H., Myhre, G., Forster, P.M., Hodnebrog, Ø., Andrews, T., Boucher, O., Faluvegi, G., Iversen, T., Kasoar, M., et al. (2017). Rapid Adjustments Cause Weak Surface Temperature Response to Increased Black Carbon Concentrations. J. Geophys. Res. Atmos. *Volume*, 11462–11481. https://doi.org/10.1002/2017JD027326.

32. Koch, D., and Del Genio, A.D. (2010). Black carbon semi-direct effects on cloud cover: review and synthesis. Atmos. Chem. Phys. *10*, 7685–7696. https://doi.org/10.5194/acp-10-7685-2010.

33. Johnson, B.T., Shine, K.P., and Forster, P.M. (2004). The semi-direct aerosol effect: Impact of absorbing aerosols on marine stratocumulus. Q. J. R. Meteorol. Soc. *130*, 1407–1422. https://doi.org/10.1256/qj.03.61.

34. Herbert, R.J., Bellouin, N., Highwood, E.J., and Hill, A.A. (2020). Diurnal cycle of the semi-direct effect from a persistent absorbing aerosol layer over marine stratocumulus in large-eddy simulations. Atmos. Chem. Phys. *20*, 1317–1340. https://doi.org/10.5194/acp-20-1317-2020.

35. Zhou, X., Ackerman, A.S., Fridlind, A.M., Wood, R., and Kollias, P. (2017). Impacts of solar-absorbing aerosol layers on the transition of stratocumulus to trade cumulus clouds. Atmos. Chem. Phys. *17*, 12725–12742. https://doi.org/10.5194/acp-17-12725-2017.

36. Gordon, H., Field, P.R., Abel, S.J., Dalvi, M., Grosvenor, D.P., Hill, A.A., Johnson, B.T., Miltenberger, A.K., Yoshioka, M., and Carslaw, K.S. (2018). Large simulated radiative effects of smoke in the south-east Atlantic. Atmos. Chem. Phys. *18*, 15261–15289. https://doi.org/10.5194/acp-18-15261-2018.

37. Brioude, J., Cooper, O.R., Feingold, G., Trainer, M., Freitas, S.R., Kowal, D., Ayers, J.K., Prins, E., Minnis, P., McKeen, S.A., et al. (2009). Effect of biomass burning on marine stratocumulus clouds off the California coast. Atmos. Chem. Phys. *9*, 8841–8856. https://doi.org/10.5194/acp-9-8841-2009.

38. Koren, I., Martins, J.V., Remer, L.A., and Afargan, H. (2008). Smoke invigoration versus inhibition of clouds over the Amazon. Science *321*, 946–949. https://doi.org/10.1126/science.1159185.

39. Richardson, T.B., Forster, P.M., Smith, C.J., Maycock, A.C., Wood, T., Andrews, T., Boucher, O., Faluvegi, G., Fläschner, D., Hodnebrog, Ø., et al. (2019). Efficacy of Climate Forcings in PDRMIP Models. J. Geophys. Res. Atmos. *124*, 12824–12844. https://doi.org/10.1029/2019JD030581.

40. Sherwood, S.C., Bony, S., Boucher, O., Bretherton, C., Forster, P.M., Gregory, J.M., and Stevens, B. (2015). Adjustments in the Forcing-Feedback Framework for Understanding Climate Change. Bull. Am. Meteorol. Soc. *96*, 217–228. https://doi.org/10.1175/BAMS-D-13-00167.1.

41. Samset, B.H., Myhre, G., Forster, P.M., Hodnebrog, Ø., Andrews, T., Faluvegi, G., Fläschner, D., Kasoar, M., Kharin, V., Kirkevåg, A., et al. (2016). Fast and slow precipitation responses to individual climate forcers: A PDRMIP multimodel study. Geophys. Res. Lett. *43*, 2782–2791. https://doi.org/10.1002/2016GL068064.

42. Chen, C., Dubovik, O., Schuster, G.L., Chin, M., Henze, D.K., Lapyonok, T., Li, Z., Derimian, Y., and Zhang, Y. (2022). Multi-angular polarimetric remote sensing to pinpoint global aerosol absorption and direct radiative forcing. Nat. Commun. *13*, 7459. https://doi.org/10.1038/s41467-022-35147-y.

43. Myhre, G., Kramer, R.J., Smith, C.J., Hodnebrog, Ø., Forster, P., Soden, B. J., Samset, B.H., Stjern, C.W., Andrews, T., Boucher, O., et al. (2018). Quantifying the Importance of Rapid Adjustments for Global Precipitation Changes. Geophys. Res. Lett. *45*, 11399–11405. https://doi.org/10.1029/2018GL079474.

44. Soden, B.J., Held, I.M., Colman, R., Shell, K.M., Kiehl, J.T., and Shields, C. A. (2008). Quantifying Climate Feedbacks Using Radiative Kernels. J. Clim. *21*, 3504–3520. https://doi.org/10.1175/2007JCLI2110.1.

45. Hodnebrog, Ø., Myhre, G., and Samset, B.H. (2014). How shorter black carbon lifetime alters its climate effect. Nat. Commun. *5*, 5065. https://doi.org/10.1038/ncomms6065.

46. Samset, B.H., Myhre, G., Schulz, M., Balkanski, Y., Bauer, S., Berntsen, T. K., Bian, H., Bellouin, N., Diehl, T., Easter, R.C., et al. (2013). Black carbon vertical profiles strongly affect its radiative forcing uncertainty. Atmos. Chem. Phys. *13*, 2423–2434. https://doi.org/10.5194/acp-13-2423-2013.

47. Zarzycki, C.M., and Bond, T.C. (2010). How much can the vertical distribution of black carbon affect its global direct radiative forcing? Geophys. Res. Lett. *37*, L20807. https://doi.org/10.21029/22010gl044555.

48. Sand, M., Samset, B.H., Tsigaridis, K., Bauer, S.E., and Myhre, G. (2020). Black Carbon and Precipitation: An Energetics Perspective. JGR Atmospheres *125*, JD032239, e2019. https://doi.org/10.1029/2019JD032239.

49. Myhre, G., Forster, P.M., Samset, B.H., Hodnebrog, Ø., Sillmann, J., Aalbergsjø, S.G., Andrews, T., Boucher, O., Faluvegi, G., Fläschner, D., et al. (2017). PDRMIP: A Precipitation Driver and Response Model Intercomparison Project—Protocol and Preliminary Results. Bull. Am. Meteorol. Soc. *98*, 1185–1198. https://doi.org/10.1175/bams-d-16-0019.1.

50. Thornhill, G.D., Collins, W.J., Kramer, R.J., Olivié, D., Skeie, R.B., O'Connor, F.M., Abraham, N.L., Checa-Garcia, R., Bauer, S.E., Deushi, M., et al. (2021). Effective radiative forcing from emissions of reactive gases and aerosols – a multi-model comparison. Atmos. Chem. Phys. *21*, 853–874. https://doi.org/10.5194/acp-21-853-2021.

51. Forster, P.M., Richardson, T., Maycock, A.C., Smith, C.J., Samset, B.H., Myhre, G., Andrews, T., Pincus, R., and Schulz, M. (2016). Recommendations for diagnosing effective radiative forcing from climate models for CMIP6. JGR Atmospheres *121*, 12460–12475. https://doi.org/10.1002/2016JD025320.

52. Myhre, G., Samset, B.H., Schulz, M., Balkanski, Y., Bauer, S., Berntsen, T. K., Bian, H., Bellouin, N., Chin, M., Diehl, T., et al. (2013). Radiative forcing of the direct aerosol effect from AeroCom Phase II simulations. Atmos. Chem. Phys. *13*, 1853–1877. https://doi.org/10.5194/acp-13-1853-2013.

53. Bond, T.C., Streets, D.G., Yarber, K.F., Nelson, S.M., Woo, J.H., and Klimont, Z. (2004). A technology-based global inventory of black and organic carbon emissions from combustion. J. Geophys. Res. *109*, D14203. https://doi.org/10.1029/2003JD003697.

54. Zhao, W., Zhao, Y., Zheng, Y., Chen, D., Xin, J., Li, K., Che, H., Li, Z., Ma, M., and Hang, Y. (2024). Long-term variability in black carbon emissions constrained by gap-filled absorption aerosol optical depth and associated premature mortality in China. Atmos. Chem. Phys. *24*, 6593–6612. https://doi.org/10.5194/acp-24-6593-2024.

55. Klimont, Z., Kupiainen, K., Heyes, C., Purohit, P., Cofala, J., Rafaj, P., Borken-Kleefeld, J., and Schöpp, W. (2017). Global anthropogenic emissions of particulate matter including black carbon. Atmos. Chem. Phys. *17*, 8681–8723. https://doi.org/10.5194/acp-17-8681-2017.

56. Stohl, A., Aamaas, B., Amann, M., Baker, L.H., Bellouin, N., Berntsen, T.K., Boucher, O., Cherian, R., Collins, W., Daskalakis, N., et al. (2015). Evaluating the climate and air quality impacts of short-lived pollutants. Atmos. Chem. Phys. *15*, 10529–10566. https://doi.org/10.5194/acp-15-10529-2015.

**CRSUS, Volume *2***

## Supplemental information

# The warming effect of black carbon

# must be reassessed

# in light of observational constraints

**Gunnar Myhre, Bjørn H. Samset, Camilla Weum Stjern, Øivind Hodnebrog, Ryan Kramer, Chris Smith, Timothy Andrews, Olivier Boucher, Greg Faluvegi, Piers M. Forster, Trond Iversen, Alf Kirkevåg, Dirk Olivié, Drew Shindell, Philip Stier, and Duncan Watson-Parris**

# Supplementary:

**Supplementary Table S1:** A selected set of measured mass absorption coefficients (MAC) given at 550 nm and original provided wavelength. Conversion of MAC to 550 nm is performed assuming absorption Ångstrøm exponent to be 1. If no value is given for original wavelength the measurements is taken at 550 nm. Regions of measurements are given along with references for measurements.

| **Location** | **MAC [$m^2$ $g^{-1}$] (550)** | **MAC [$m^2$ $g^{-1}$] at reported wavelength** | **Reference** |
|---|---|---|---|
| Large set of data | 7.5 ± 1.2 and 11 $m^2$ $g^{-1}$ at 550 nm for fresh and aged BC particles | | Bond and Bergstrom [1] |
| Urban | 6.8 – 8.7 | | Hitzenberger et al. [2] |
| Mexico City | 8.7 – 8.9 | 5.5 – 5.6 (870)[1] | Doran et al. [3] |
| Mexico | 13.1 | 10.9 (660) | Subramanian et al. [4] |
| High altitude (winter)<br>High altitude (summer) | 8.6<br>12.7 | 7.5 (630)<br>11 (630) | Cozic et al. [5] |
| Denver | 9.7 | 10 (532)[2] | Knox et al. [6] |
| Different sites in India | 7.4 – 17.3 | Between 6 and 14 (at 678 nm) | Ram and Sarin [7] |
| Urban (Barcelona)<br>Traffic (Bern)<br>Industrial (Huelva) | 10.7<br>11.9<br>11.4 | 9.2 (637)<br>10.3 (637)<br>9.8 (637) | Reche et al. [8] |
| Urban (Paris) | 13.8 | 8.6 (880) | Laborde et al. [9] |
| Shenzhen (China) | 6.3 | 6.5 ± 0.5 (532) | Lan et al. [10] |
| South Texas | 7.8 | 8.1 (532) | Levy et al. [11] |
| Arctic | 5.7 | around 6 (522 nm) | Yttri et al. [12] |
| Rural North China | 12.3 | 10 (678 nm) | Cui et al. [13] |
| Aspvreten (SE)<br>Birkenes (NO<br>Finokalia (GR)<br>Harwell (GB)<br>Ispra (IT)<br>Melpitz (DE)<br>Montseny (ES)<br>Puy de Dôme (FR)<br>Vavihill (SE) | 9.8<br>9.1<br>14.3<br>15.6<br>11.1<br>10.7<br>10.3<br>20.0<br>7.5 | 8.51 (637)<br>7.86 (637)<br>12.4 (637)<br>13.5 (637)<br>9.61 (637)<br>9.23 (637)<br>8.92 (637)<br>17.3 (637)<br>6.47(637) | Zanatta et al. [14] |
| Fresno, Italy | 7.4 | 7.9 ± 1.5 (532) | Presler-Jur et al. [15] |
| Northwest China | 13.3 | 8.3 (880) as an average of 7.4, 5.7, 8.1 and 12.1 | Zhang et al. [16] |
| Milan, Italy | 9.9 | 10.2 (532) | Forello et al. [17] |
| China | 11.4 | 11.8 (532) | Ma et al. [18] |
| Bangladesh<br>Maldives | 5.2 ± 1.7<br>8.7 ± 1.8 to 9.7 ±2.3 | 4.2 ± 1.4<br>7.1 ± 1.5 to 7.9 ± 1.9 | Nair et al. [19] |

[1] See correction of the publication.
[2] See value provided in Ma et al. (2020).

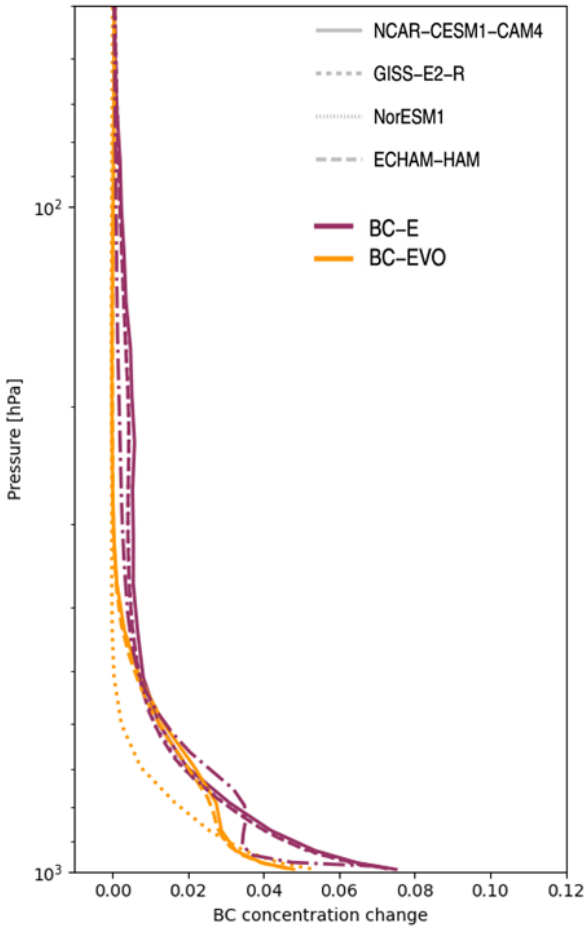


**Supplementary Figure S1:** Atmospheric vertical profile of black carbon, for the 2 BC experiments BC-E and BC-EVO. The standard vertical profile is shown in purple and vertical constrained in orange. Note the strong reduction in BC concentration at higher altitudes in the troposphere in the observationally constrained profiles. Some of the lines are overlayed in the concentration driven models.

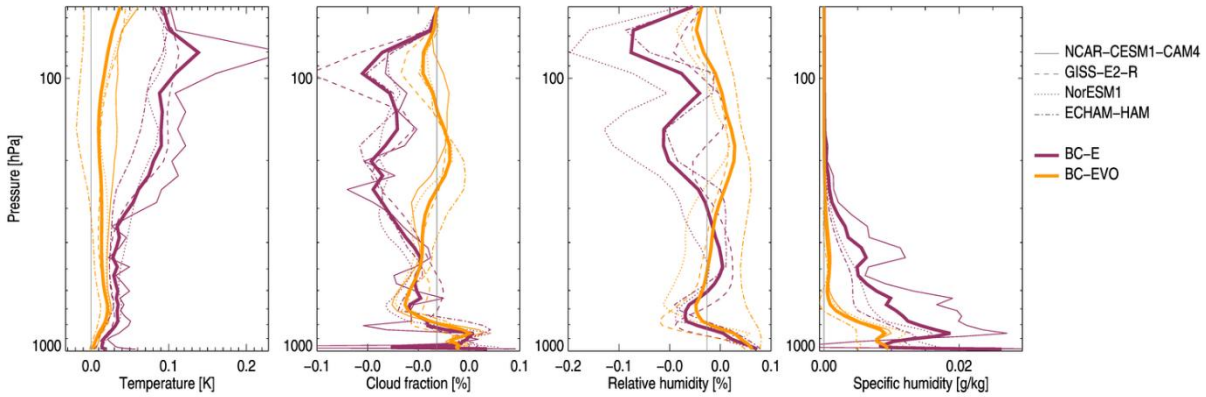


**Supplementary Figure S2:** Like Figure 4 but showing the results from each of the four models. Atmospheric vertical profiles of changes in temperature, cloud fraction, relative humidity, and specific humidity for the two experiments BC-E and BC-EVO.

**Supplementary Note S1:** In Figure S1, we decompose IRF, rapid adjustments and ERF into shortwave (SW) and longwave (LW) radiation components (only shown for BC-E and BC-EVO). The SW and LW ERF are direct output from the model simulations, whereas IRF and rapid adjustment terms are derived using the same approach as in Figure 1 (see Methods). The IRF is almost solely a result of BC interacting with SW radiation. Note, however, that two of the four models have a very weak LW IRF effect in the simulations. The total rapid adjustment mainly affects the LW radiation. Looking into the radiative distribution of the individual rapid adjustment terms (not shown), the temperature rapid adjustment terms impact LW radiation only, and water vapor and clouds also mostly impact the LW radiation. LW rapid adjustment from clouds and water vapor are up to half of the total LW rapid adjustment in magnitude but their rapid adjustment terms are of opposite sign. Similarly, SW rapid adjustments for clouds are negative and those for water vapor are positive. Because of these compensating terms, the total SW rapid adjustment varies in sign across the models. The net radiation changes behind the rapid adjustment in Figure 1 are very different for the two experiments, and it can be seen in Fig. S1 that this originates from differences in LW radiation. Supplementary Figure S2 shows the residuals in the rapid adjustment calculations. Residuals can be derived due to the availability of double-radiation calls and because BC induced changes in LW radiation are almost entirely due to rapid adjustments. The residuals are particularly small for net (LW + SW) rapid adjustment. As uncertainties in the kernel simulations of temperature and water vapor changes are relatively small [20], this further indicates that residuals in the cloud rapid adjustment calculations are small.

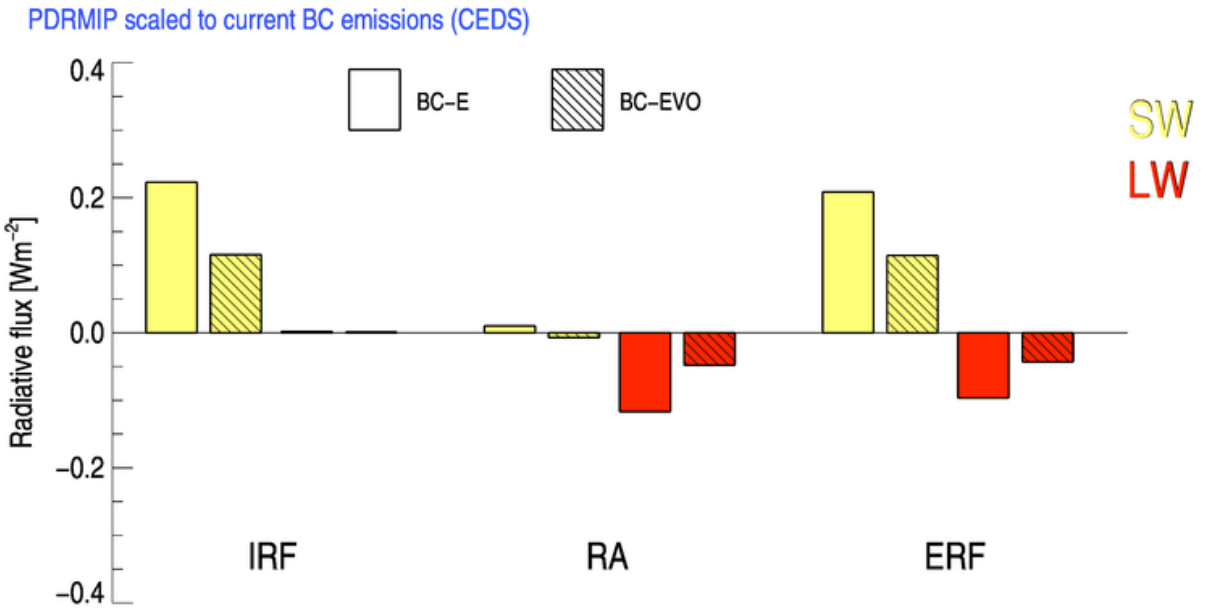


**Supplementary Figure S3:** Global mean instantaneous radiative forcing (IRF), rapid adjustments (RA), effective radiative forcing (ERF) divided into longwave (LW) and shortwave (SW) radiation from the two experiments BC-E (full bars) and BC-EVO (bars with lines). Net values (SW + LW) are shown in Figure 2.

**Supplementary Note S2:** We have provided results from the fully coupled climate models from year 51-100 but also gave an estimate for year 20 (mean of year 18-22). The rationale for looking at year 20 is that a zero layer model provides a good fit to the historical record (e.g., Gregory and Forster [21,]Held et al. [22]). In step change experiments the upper-layer has approximately come into equilibrium at about year 20, while the deep-ocean can still be approximated as dT ~ 0 (in a two-layer ocean model, representing the mixed-layer and deep-ocean). This is further described in Section 3 of Gregory et al. [23].

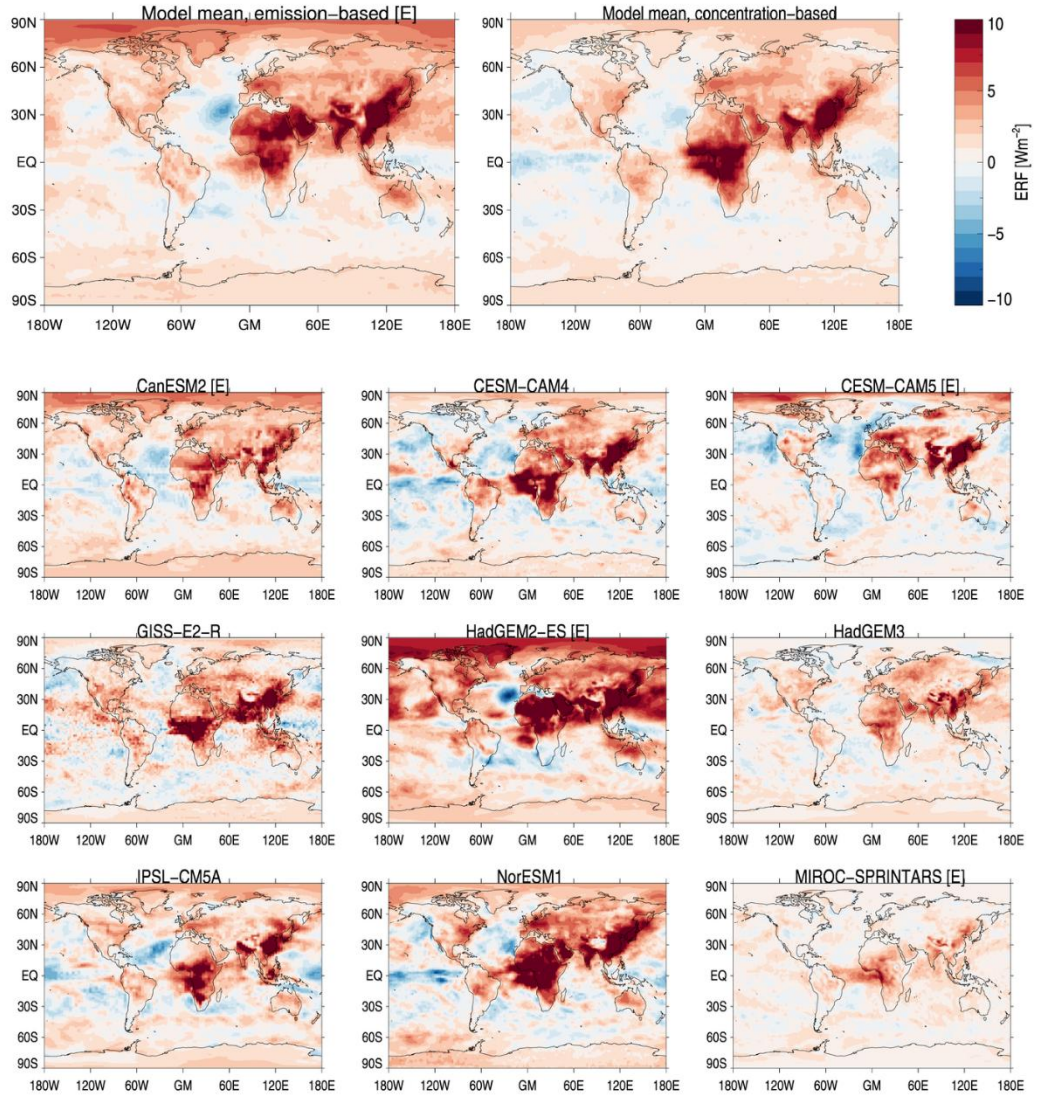


**Supplementary Figure S4:** ERF for PDRMIP BC experiment for 9 PDRMIP models shown in Stjern et al. [24] and models mean for emission driven and concentration driven models. All models are scaled to the same emissions as for the concentration driven models and given for BCx10.

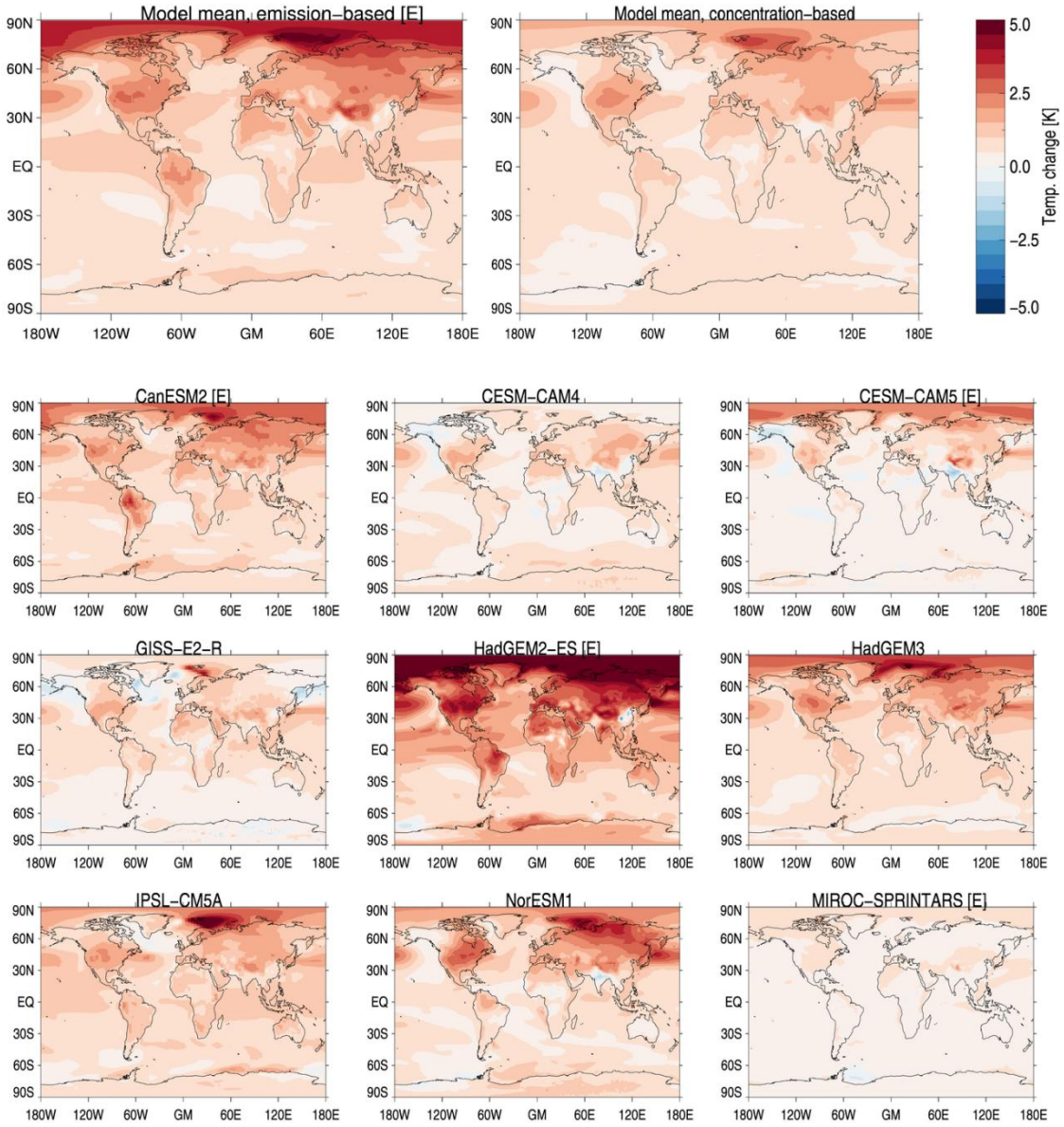


**Supplementary Figure S5:** Surface temperature change for the PDRMIP BC experiment for 9 PDRMIP models shown in Stjern *et al.* [24], and model means for emission driven and concentration driven models. All models are scaled to the same emissions as for the concentration driven models and given for BCx10.

**Supplementary Table S2:** Global and annual mean effective radiative forcing (ERF), ERF normalized by absorption aerosol optical depth (AAOD), ERF normalized by burden, and temperature change for PDRMIP BC experiment for 9 PDRMIP models [24]. The ECHAM-HAM results are performed for this study. Results are provided for emission driven and concentration driven models. All models are scaled to the same emissions as for the concentration driven models. Note that all results are for 10xBC and there is no scaling by mass absorption coefficient.

| | **ERF [$Wm^{-2}$]** | **Normalized ERF [$Wm^{-2}$]** | **Norm, ERF [$Wg^{-1}$]** | **Emission-scaled temp, change [K]** |
|---|---|---|---|---|
| **CanESM2 [E]** | 1.54 | NA | 350 | 0.78 |
| **CESM-CAM5 [E]** | 0.41 | 49 | 490 | 0.17 |
| **HadGEM2-ES [E]** | 2.91 | 153 | 490 | 1.51 |
| **MIROC-SPRINTARS [E]** | 0.65 | 81 | 330 | 0.11 |
| **GISS-E2-R** | 1.26 | 112 | 640 | 0.39 |
| **CESM-CAM4** | 0.78 | 59 | 430 | 0.35 |
| **HadGEM3** | 0.68 | 70 | 380 | 0.70 |
| **IPSL-CM5A** | 0.82 | 76 | 440 | 0.75 |
| **NorESM1** | 1.43 | 100 | 750 | 0.67 |
| **ECHAM-HAM** | 0.73 | 58 | NA | 0.24 |

**Supplementary Table S3:** Multi-model global and annual mean instantaneous radiative forcing (IRF), effective radiative forcing (ERF), rapid adjustment, surface temperature for the BC-E and BC-EVO experiments. Numbers in parentheses are one standard deviation from the four models in this study. Results are shown for CEDS emission versions from 2024 and 2016 (applied in CMIP6).

| **CEDS Emissions v2024** | | |
|---|---|---|
| | BC-E | BC-EVO |
| IRF | 0.22 (0.01) | 0.13 (0.02) |
| ERF | 0.11 (0.04) | 0.07 (0.05) |
| Rapid adjustments | -0.11 (0.03) | -0.06 (0.03) |
| Surface temperature change | 0.05 (0.02) | 0.02 (0.02) |
| **CEDS Emissions v2016** | | |
| IRF | 0.35 (0.02) | 0.20 (0.03) |
| ERF | 0.17 (0.06) | 0.11 (0.06) |
| Rapid adjustments | -0.16 (0.06) | -0.08 (0.05) |
| Surface temperature change | 0.07 (0.03) | 0.04 (0.03) |

**Supplementary Note S3:** Since the rapid adjustments are derived using kernel techniques it is important to assess the uncertainties in the calculations. In particular, the residuals provide information on the clouds rapid adjustments, where uncertainties are larger than for the other contributors according to Smith *et al.* [20]. The residual between direct model output and calculations using radiative kernels are shown in Figure S2 for model mean and individual models, and for SW, LW and Net. Since SW and LW residuals are of opposite sign, the net residuals are weakest, indicating that uncertainties are small in the rapid adjustment calculations shown in Figure 1. Residuals are stronger in magnitude in absolute and relative terms in BC-E compared to the BC-EVO experiment. The residuals are well within the model range for the total rapid adjustment shown in Figure 1 in the main manuscript. Maximum model range in the residual is 0.03 W $m^{-2}$ for LW rapid adjustments. Residuals are possible to quantify for all four models for LW radiation using ERF, but for SW radiation this is available only for the three models which performed double radiation calls.

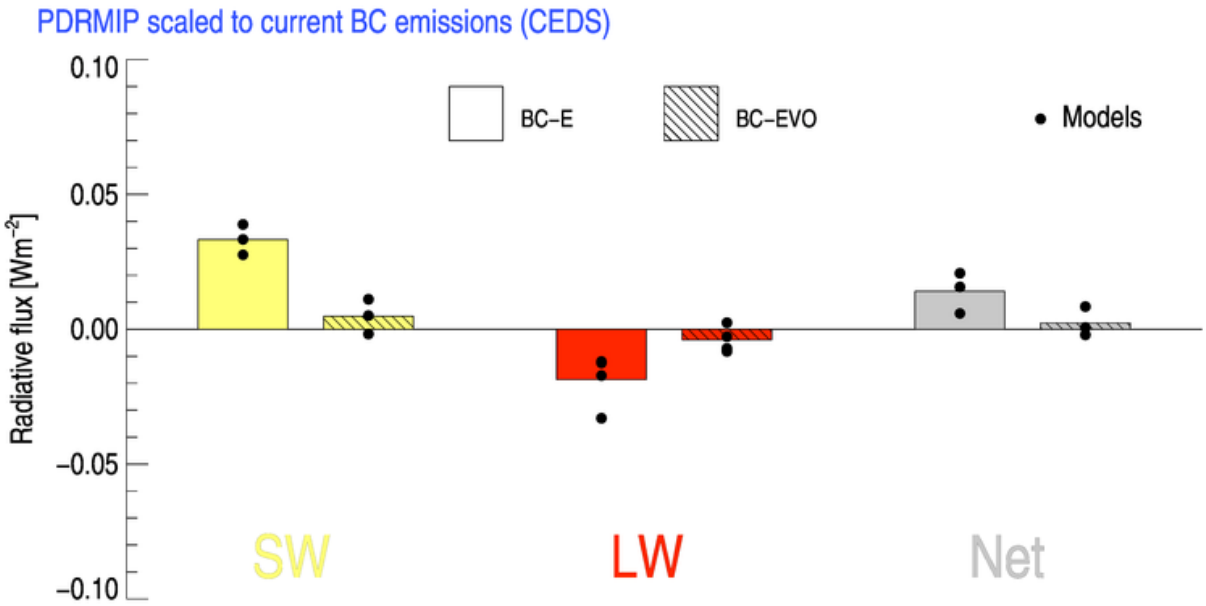


**Supplementary Figure S6:** Global mean residuals between direct climate model results and radiative kernel calculations of rapid adjustments, divided into longwave (LW), shortwave (SW) and Net radiation from the two experiments BC-E (full bars) and BC-EVO (bars with lines). Individual models are shown as black dots. Three models have double radiation calls allowing derivation of residual for SW and Net. Residual between radiative kernel calculations and climate model results of rapid adjustment is derived from LW ERF since LW IRF is either zero or derived by double radiative calls.

**References:**


1. Bond, T.C., and Bergstrom, R.W. (2006). Light absorption by carbonaceous particles: An investigative review. Aerosol Science And Technology *40*, 27-67.
2. Hitzenberger, R., Petzold, A., Bauer, H., Ctyroky, P., Pouresmaeil, P., Laskus, L., and Puxbaum, H. (2006). Intercomparison of Thermal and Optical Measurement Methods for Elemental Carbon and Black Carbon at an Urban Location. Environmental Science & Technology *40*, 6377-6383. 10.1021/es051228v.
3. Doran, J.C., Barnard, J.C., Arnott, W.P., Cary, R., Coulter, R., Fast, J.D., Kassianov, E.I., Kleinman, L., Laulainen, N.S., Martin, T., et al. (2007). The T1-T2 study: evolution of aerosol properties downwind of Mexico City. Atmos. Chem. Phys. *7*, 1585-1598. 10.5194/acp-7-1585-2007.
4. Subramanian, R., Kok, G.L., Baumgardner, D., Clarke, A., Shinozuka, Y., Campos, T.L., Heizer, C.G., Stephens, B.B., de Foy, B., Voss, P.B., and Zaveri, R.A. (2010). Black carbon over Mexico: the effect of atmospheric transport on mixing state, mass absorption cross-section, and BC/CO ratios. Atmos. Chem. Phys. *10*, 219-237. 10.5194/acp-10-219-2010.
5. Cozic, J., Verheggen, B., Weingartner, E., Crosier, J., Bower, K.N., Flynn, M., Coe, H., Henning, S., Steinbacher, M., Henne, S., et al. (2008). Chemical composition of free tropospheric aerosol for PM1 and coarse mode at the high alpine site Jungfraujoch. Atmos. Chem. Phys. *8*, 407-423. 10.5194/acp-8-407-2008.
6. Knox, A., Evans, G.J., Brook, J.R., Yao, X., Jeong, C.H., Godri, K.J., Sabaliauskas, K., and Slowik, J.G. (2009). Mass Absorption Cross-Section of Ambient Black Carbon Aerosol in Relation to Chemical Age. Aerosol Science and Technology *43*, 522-532. 10.1080/02786820902777207.
7. Ram, K., and Sarin, M.M. (2009). Absorption Coefficient and Site-Specific Mass Absorption Efficiency of Elemental Carbon in Aerosols over Urban, Rural, and High-Altitude Sites in India. Environmental Science & Technology *43*, 8233-8239. 10.1021/es9011542.
8. Reche, C., Querol, X., Alastuey, A., Viana, M., Pey, J., Moreno, T., Rodríguez, S., González, Y., Fernández-Camacho, R., de la Rosa, J., et al. (2011). New considerations for PM, Black Carbon and particle number concentration for air quality monitoring across different European cities. Atmos. Chem. Phys. *11*, 6207-6227. 10.5194/acp-11-6207-2011.
9. Laborde, M., Crippa, M., Tritscher, T., Jurányi, Z., Decarlo, P.F., Temime-Roussel, B., Marchand, N., Eckhardt, S., Stohl, A., Baltensperger, U., et al. (2013). Black carbon physical properties and mixing state in the European megacity Paris. Atmos. Chem. Phys. *13*, 5831-5856. 10.5194/acp-13-5831-2013.
10. Lan, Z.-J., Huang, X.-F., Yu, K.-Y., Sun, T.-L., Zeng, L.-W., and Hu, M. (2013). Light absorption of black carbon aerosol and its enhancement by mixing state in an urban atmosphere in South China. Atmos. Environ. *69*, 118-123. https://doi.org/10.1016/j.atmosenv.2012.12.009.
11. Levy, M.E., Zhang, R., Khalizov, A.F., Zheng, J., Collins, D.R., Glen, C.R., Wang, Y., Yu, X.-Y., Luke, W., Jayne, J.T., and Olaguer, E. (2013). Measurements of submicron aerosols in Houston, Texas during the 2009 SHARP field campaign. J. Geophys. Res. - Atmos. *118*, 10,518-510,534. 10.1002/jgrd.50785.
12. Yttri, K.E., Lund Myhre, C., Eckhardt, S., Fiebig, M., Dye, C., Hirdman, D., Ström, J., Klimont, Z., and Stohl, A. (2014). Quantifying black carbon from biomass burning by means of levoglucosan – a one-year time series at the Arctic observatory Zeppelin. Atmos. Chem. Phys. *14*, 6427-6442. 10.5194/acp-14-6427-2014.
13. Cui, X., Wang, X., Yang, L., Chen, B., Chen, J., Andersson, A., and Gustafsson, Ö. (2016). Radiative absorption enhancement from coatings on black carbon aerosols. Science of The Total Environment *551–552*, 51-56. http://dx.doi.org/10.1016/j.scitotenv.2016.02.026.
14. Zanatta, M., Gysel, M., Bukowiecki, N., Müller, T., Weingartner, E., Areskoug, H., Fiebig, M., Yttri, K.E., Mihalopoulos, N., Kouvarakis, G., et al. (2016). A European aerosol phenomenology-5: Climatology of black carbon optical properties at 9 regional background

sites across Europe. Atmos. Environ. *145*, 346-364. https://doi.org/10.1016/j.atmosenv.2016.09.035.
15. Presler-Jur, P., Doraiswamy, P., Hammond, O., and Rice, J. (2017). An evaluation of mass absorption cross-section for optical carbon analysis on Teflon filter media. Journal of the Air & Waste Management Association *67*, 1213-1228. 10.1080/10962247.2017.1310148.
16. Zhang, Q., Shen, Z., Lei, Y., Zhang, T., Zeng, Y., Ning, Z., Sun, J., Westerdahl, D., Xu, H., Wang, Q., et al. (2019). Optical properties and source identification of black carbon and brown carbon: comparison of winter and summer haze episodes in Xi'an, Northwest China. Environmental Science: Processes & Impacts *21*, 2058-2069. 10.1039/C9EM00320G.
17. Forello, A.C., Bernardoni, V., Calzolai, G., Lucarelli, F., Massabò, D., Nava, S., Pileci, R.E., Prati, P., Valentini, S., Valli, G., and Vecchi, R. (2019). Exploiting multi-wavelength aerosol absorption coefficients in a multi-time resolution source apportionment study to retrieve source-dependent absorption parameters. Atmos. Chem. Phys. *19*, 11235-11252. 10.5194/acp-19-11235-2019.
18. Ma, Y., Huang, C., Jabbour, H., Zheng, Z., Wang, Y., Jiang, Y., Zhu, W., Ge, X., Collier, S., and Zheng, J. (2020). Mixing state and light absorption enhancement of black carbon aerosols in summertime Nanjing, China. Atmos. Environ. *222*, 117141. https://doi.org/10.1016/j.atmosenv.2019.117141.
19. Nair, H.R.C.R., Budhavant, K., Manoj, M.R., Kirillova, E.N., Satheesh, S.K., and Gustafsson, Ö. (2024). Roles of water-soluble aerosol coatings for the enhanced radiative absorption of black carbon over south asia and the northern indian ocean. Science of The Total Environment *926*, 171721. https://doi.org/10.1016/j.scitotenv.2024.171721.
20. Smith, C.J., Kramer, R.J., Myhre, G., Forster, P.M., Soden, B.J., Andrews, T., Boucher, O., Faluvegi, G., Fläschner, D., Hodnebrog, Ø., et al. (2018). Understanding Rapid Adjustments to Diverse Forcing Agents. Geophys. Res. Lett. *45*, 12023-12031. 10.1029/2018gl079826.
21. Gregory, J.M., and Forster, P.M. (2008). Transient climate response estimated from radiative forcing and observed temperature change. J. Geophys. Res.-Atmos. *113*, D23105, D23105. 10.1029/2008jd010405.
22. Held, I.M., Winton, M., Takahashi, K., Delworth, T., Zeng, F., and Vallis, G.K. (2010). Probing the Fast and Slow Components of Global Warming by Returning Abruptly to Preindustrial Forcing. J. Climate *23*, 2418-2427. 10.1175/2009jcli3466.1.
23. Gregory, J.M., Andrews, T., and Good, P. (2015). The inconstancy of the transient climate response parameter under increasing CO<sub>2</sub>. Philosophical Transactions of the Royal Society A: Mathematical, Physical and Engineering Sciences *373*, 20140417. doi:10.1098/rsta.2014.0417.
24. Stjern, C.W., Samset, B.H., Myhre, G., Forster, P.M., Hodnebrog, Ø., Andrews, T., Boucher, O., Faluvegi, G., Iversen, T., Kasoar, M., et al. (2017). Rapid Adjustments Cause Weak Surface Temperature Response to Increased Black Carbon Concentrations. J. Geophys. Res. - Atmos. *122*, 11462-11481. 10.1002/2017JD027326.